Single-section multiplexed imaging enables comprehensive lung cancer diagnosis

Raz Ben-Uri[1*], Tal Keidar Haran[1,2*#], Yuval Bussi[1,3], Gilad Vainer[2], Johnathan Arnon[4], Nir Pillar[2], Hasan Sourikh[2], Inbal Fuchs[4], Ofer Elhanani[1], Tzahi Neuman[2], Eli Pikarsky[2,5], Leeat Keren[1#]

Abstract

Accurate and timely diagnosis is essential for effective lung cancer treatment. However, contemporary diagnostic workflows rely on sequential immunohistochemistry of small biopsy specimens, which can exhaust limited tissue, compromise diagnostic accuracy, and delay treatment decisions with clinical consequences. Here, we demonstrate that multiplexed imaging overcomes these limitations by enabling comprehensive lung cancer diagnosis from a single tissue section. We developed and validated a clinically informed multiplexed antibody panel that integrates tumor diagnosis and classification, predictive biomarker assessment, and tumor immune profiling. In diagnostic biopsies, multiplexed imaging achieved 96% concordance with standard pathological diagnosis, while enabling accurate automated PD-L1 scoring and rapid detection of clinically approved and emerging actionable targets. This approach preserves scarce tissue, supports quantitative computational analysis to streamline diagnosis, and generates research-grade spatial data while accelerating diagnostic workflow. Together, these findings establish multiplexed imaging as a robust, time and tissue-efficient framework for lung cancer diagnostics that bridges clinical care and translational discovery.

1. Department of Molecular Cell Biology, Weizmann Institute of Science, Israel
2. Department of Pathology, Hadassah Hebrew University Medical Center, Jerusalem, Israel
3. Department of Mathematics and Computer Science, Weizmann Institute of Science, Israel
4. Sharett Institute of Oncology, Hadassah Hebrew University Medical Center, Jerusalem, Israel
5. The Lautenberg Center for Immunology and Cancer Research, Hebrew University of Jerusalem, Israel

* Equal contribution

\# Corresponding authors: talkeidar@hadassah.org.il , leeat.keren@weizmann.ac.il

Introduction

Lung cancer is the leading cause of cancer-related mortality worldwide, with approximately 2.5 million new cases and over 1.8 million deaths reported annually [1]. However, therapeutic advances over the past two decades have markedly improved outcomes for selected patient populations. Targeted therapies, such as inhibitors of epidermal growth factor receptor (EGFR) or anaplastic lymphoma kinase (ALK), and immune-based treatments, most notably inhibitors of programmed cell death protein 1 (PD-1) or its ligand (PD-L1), have demonstrated remarkable improvements in clinical outcomes [2–8]. Because effectiveness of these therapies depends on the distinct features of an individual's tumor, optimizing patient outcomes increasingly relies on timely and accurate diagnostic assessment. At the same time, refined classification and the growing number of actionable biomarkers have rendered the diagnostic process progressively more complex [9–11].

Contemporary lung cancer diagnostics favor minimally invasive biopsy approaches to minimize patient risk, a shift that has improved procedural safety while simultaneously increasing reliance on small biopsy specimens. Biopsies are used to establish malignancy and tumor origin, determine histologic subtype, and initiate molecular testing that informs staging and treatment planning. To ensure sufficient tissue for downstream analyses, the diagnostic workflow proceeds through a sequential pipeline, beginning with standard hematoxylin and eosin (H&E) staining and immunohistochemistry (IHC) for tumor classification. Histopathological evaluation distinguishes primary lung cancer from other thoracic malignancies or metastatic lesions, separates small cell lung cancer (SCLC) from non-small cell lung cancer (NSCLC), and further subtypes NSCLC into adenocarcinoma, squamous cell carcinoma, and less common variants [12,13]. These distinctions are clinically essential, as therapeutic strategies and responses differ substantially across subtypes [14]. Subsequently, tissues are tested for predictive biomarkers such as PD-L1 expression and ALK rearrangements, through additional IHC stains and then undergo additional molecular assays, typically by next-generation sequencing (NGS) panels [15,16].

While this stepwise approach is well established, it is poorly suited to the realities of small diagnostic biopsies which are common in thoracic malignancies (e.g. transbronchial and endobronchial biopsies) and clinical decision making. As the current workflow is based on one stain per section, it is inherently tissue-depleting, slow and suboptimal, with profound consequences for patient care. In complex cases, a single biopsy may undergo up to 20 serial stains, rapidly exhausting the limited material available [12]. As each diagnostic test consumes additional tissue, many specimens are depleted before critical biomarkers such as PD-L1, EGFR and ALK can be evaluated. As a result, approximately one in five biopsies is ultimately insufficient for a complete molecular workup [14,17], necessitating repeat invasive biopsies that increase patient risk and delay therapy initiation. These delays are particularly

consequential given that most lung cancer patients present with advanced or metastatic disease, where rapid and well-informed treatment decisions are essential for survival. Crucially, up to 25% of patients die within 1-3 months of diagnosis, often before a full diagnostic evaluation is completed or treatment is initiated (**Fig. 1A**) [18–23]. Accordingly, implementing faster diagnostic workflows in this clinical setup can be lifesaving.

Beyond delays, the current diagnostic workflow presents challenges related to accuracy and translational utility. Because IHC stains are performed on separate serial sections, pathologists must integrate information across slides that are not perfectly aligned. This limitation is exemplified in PD-L1 scoring, which is based on the percentage of viable tumor cells exhibiting membranous PD-L1 staining. In current workflows, pathologists score PD-L1 on a dedicated IHC slide and rely on visual alignment with the corresponding H&E section to identify tumor cells. In challenging cases, such as biopsies with sparse tumor cells, borderline scoring or extensive inflammation, additional IHC stains may be required to delineate tumor cells. With clinically relevant PD-L1 thresholds as low as 1% guiding treatment selection, even minor shifts in tissue architecture between serial sections can introduce spatial inconsistencies that compromise scoring accuracy and influence therapeutic decision-making [15,24–26].

In addition, the tissue-depleting nature of the workflow often leaves insufficient material for molecular testing, research or participation in clinical trials, which often require specific tissue analyses for patient inclusion. This limitation has become increasingly prominent with the adoption of neoadjuvant immunotherapy. While these treatments can induce major or complete pathological responses in 20-35% of patients [27–30], they frequently leave minimal or no residual tumor in resection specimens. Conserving untreated diagnostic biopsy material for additional testing and translational research is therefore increasingly critical.

Taken together, while IHC remains essential for tumor classification and biomarker assessment [31–33], its sequential nature and excessive tissue consumption underscore the urgent need for more efficient diagnostic strategies that support biomarker complexity, maintain spatial integrity, minimize tissue exhaustion and accelerate clinical decision-making and discovery. While several works suggested to utilize serial IHC to profile a handful of markers on a single section, these endeavors lacked the scale, integration, or automation required to make an impact on clinical practices [34–36].

Here, we demonstrate the utility of multiplexed imaging technologies, which enable the simultaneous detection of dozens of markers within a single tissue section, for lung cancer diagnosis. We developed a clinically informed antibody panel incorporating markers routinely used for lung tumor subtyping and predictive biomarker evaluation. We calibrated this panel on a representative cohort of lung resections, including multiple NSCLC subtypes, SCLC, metastatic lesions and other thoracic malignancies. We

subsequently evaluated it on biopsy specimens, where it achieved 96% concordance with conventional IHC. We leveraged the high-dimensional nature of the data to perform automated cell segmentation and quantification of tumor PD-L1 expression, expediting and standardizing the analysis. We further expanded the panel to include biomarkers which are currently used to direct targeted therapies or are under clinical investigation, enabling identification of patients potentially eligible for experimental therapies within the same assay. The inclusion of additional immune-oncology markers allowed profiling of the immune tumor microenvironment (TME) in diagnostic specimens, revealing associations of distinct immune-infiltrating populations with distinct thoracic malignancies. These results illustrate how multiplexed imaging, when integrated into routine diagnostic workflows, can generate research-grade data for every patient while preserving limited tissue, seamlessly bridging clinical care with discovery. Collectively, our findings demonstrate that multiplexed imaging achieves high concordance with current diagnostic pipelines while surpassing them in tissue conservation, analytical consistency, and workflow efficiency, supporting multiplexed imaging as a practical framework for next-generation clinical diagnostics in lung cancer and beyond.

Results

Design and optimization of a multiplexed antibody panel for lung cancer diagnosis

We developed a multiplexed antibody panel for diagnostic evaluation of a broad spectrum of lung pathologies, designed to mirror the logic of the conventional clinical workflow and aligned with the guidelines of the American Society of Clinical Oncology (ASCO) and the College of American Pathologists (CAP). The panel integrates markers required to classify primary lung malignancies, such as adenocarcinoma, squamous cell carcinoma, SCLC, and mesothelioma (e.g., TTF-1, p40, CK7, Synaptophysin and INSM1), as well as lung metastases, including breast, colorectal and renal cell carcinoma (e.g., CD10, CK20). In addition, the panel included biomarkers relevant for stratification of approved therapies, including PD-L1, ALK and ROS1, as well as investigational therapies, including TROP2, and MUC1. Finally, the panel included markers for immune cell populations, phenotype and TME analysis (e.g. CD45, HLA-I, and CD3). Altogether, it enables simultaneous assessment of tumor origin, histologic subtype, and predictive biomarkers within a single staining assay (**Fig. 1B**).

We designed the assay to maximize diagnostic accuracy and compatibility with clinical workflows. We implemented it on the COMET platform, a cyclic immunofluorescence (IF) system that supports multiplexed imaging of formalin-fixed paraffin-embedded (FFPE) tissue using off-the-shelf primary antibodies and fluorescent secondary antibodies [37]. This approach enabled use of clinical antibody clones without the need for conjugation, facilitating direct translation from standard IHC. All antibodies were

individually titrated and validated on FFPE control tissues using both IHC and IF to confirm specificity, signal intensity, and appropriate subcellular localization (**Supplementary Fig. 1A**).

Next, we evaluated the assay's diagnostic performance in a controlled validation cohort. We assembled a cohort of lung resection specimens, representing the major diagnostic categories routinely encountered in clinical lung pathology. For each case, we selected representative regions of interest (ROIs), which were incorporated into a tissue microarray (TMA) and stained with the multiplexed panel (**Supplementary Fig. 1B**). A board-certified pathologist, blinded to all clinical and pathological information, reviewed the multiplexed images alongside paired H&E sections and rendered diagnoses based solely on the multiplexed data. Multiplexed-based classifications showed high concordance with the original pathology diagnosis, correctly identifying 55 of 62 cases (88%, Cohen's $\kappa = 0.85$, **Supplementary Fig. 1C-D**).

Analysis of discordant cases revealed two distinct failure modes. Four cases were misclassified due to suboptimal antibody titration, which was subsequently corrected during panel refinement. In the remaining three cases, the sections taken for multiplexed imaging no longer contained viable tumor, reflecting tumor loss during serial sectioning in the clinical diagnostic procedure. Based on the available section, these samples were correctly classified by our pathologist as containing no tumor. Excluding them from the analysis sets the concordance at 55/59 cases (93%, Cohen's $\kappa = 0.91$). Together, these results demonstrate that the multiplexed panel faithfully reproduces established diagnostic classifications in high-quality surgical specimens. They also highlight how tissue depletion inherent to serial-section workflows can directly compromise diagnostic accuracy.

Multiplexed imaging enables accurate classification of diagnostic biopsies

Following validation in resection specimens, we evaluated the performance of the multiplexed assay in routine diagnostic biopsies, where limited tissue availability and morphological ambiguity present greater challenges. We assembled a cohort of 54 biopsies (transbronchial, endobronchial and needle biopsies), obtained from patients who underwent clinical workup for suspected thoracic malignancy. The cohort encompassed a broad spectrum of pathologies encountered in clinical practice, including primary lung malignancies (adenocarcinoma, squamous cell carcinoma, small cell carcinoma, carcinoid tumors, and mesothelioma), metastatic tumors (melanoma, renal cell carcinoma, and sarcomas), as well as non-neoplastic and inflammatory conditions. Several biopsies were non-diagnostic or contained only inflammatory tissue, including confirmed cases of sarcoidosis **(Fig. 1C)**.

A single section from each biopsy was profiled using the multiplexed protocol. A board-certified pathologist, blinded to the original diagnosis and all clinical metadata, reviewed the multiplexed images

alongside the paired H&E slide and rendered a diagnosis based on marker expression and morphology (**Fig. 1C**). Multiplexed-based diagnoses were then compared with the original clinical diagnoses established using conventional H&E and IHC. Using a single tissue section per case, and blinded to the patients' clinical data, we achieved a diagnostic concordance of 96% (52/54, Cohen's κ = 0.95), including accurate classification of rare tumor subtypes and metastatic lesions (**Fig. 1D-E, Supplementary Fig. 2A**).

We identified two discordant cases and reviewed them in detail. In one case we classified a squamous cell carcinoma sample as "no tumor" since no tumor cells were present in the section used for multiplexed imaging. This reflects tumor loss during serial sectioning and underscores the value of performing all stains on a single slide to conserve material. In the second case, the original diagnosis classified the tumor as a poorly differentiated carcinoma based on weak TTF-1 staining. While multiplexed imaging confirmed weak TTF-1 expression, it also revealed strong ALK expression, an actionable alteration predominantly associated with adenocarcinoma, which led to reclassification of the tumor (**Fig. 1F**). This case demonstrates how simultaneous assessment of tumor morphology, lineage markers, and predictive biomarkers within a single assay can refine classification in diagnostically ambiguous biopsies. These results establish the capabilities of multiplexed imaging for biopsy-based lung cancer classification, motivating its application to quantitative biomarker assessment.

Multiplexed imaging enables accurate manual and automated PD-L1 scoring on a single tissue section

PD-L1 expression is a key biomarker guiding immunotherapy treatment in lung cancer and is routinely assessed by IHC using the tumor proportion score (TPS), defined as the percentage of viable tumor cells exhibiting membranous PD-L1 staining. TPS stratifies tumors into clinically relevant categories, including negative (<1%), weakly positive (1–49%), and strongly positive (≥50%). Because multiplexed imaging assesses PD-L1 on the same section used to identify tumor and immune cells, we evaluated whether our approach could reproduce TPS scoring and facilitate automated analysis.

To benchmark multiplexed imaging against clinical standards, we analyzed 31 diagnostic biopsy specimens spanning all three TPS categories based on pathological evaluation. We first performed manual TPS scoring on the multiplexed images by estimating the fraction of PD-L1–positive tumor cells, while excluding PD-L1–positive immune cells using lineage-specific markers such as CD45 and CD68 (**Fig. 2A**). To further enhance reproducibility and reduce subjectivity, we developed an automated TPS scoring pipeline based on the multiplexed data. Tumor regions were annotated to exclude tissue edges and necrotic regions, followed by single-cell segmentation using InstanSeg [38]. Two independent classifier thresholds were applied: one to identify tumor cells based on tumor-specific markers such as CK7, TTF-

1, CK5 and p40, and a second to classify PD-L1 positivity at the cellular level. The intersection of these populations yielded an automated TPS value for each sample (**Fig. 2B, Methods**). We applied this pipeline to the same cohort used for manual scoring (**Fig. 2C**).

Comparison of multiplexed-based scoring with the original clinical TPS reports demonstrated high concordance. Both manual and automated multiplexed TPS using the same thresholds matched the clinical classification in 30 of 31 cases (97% concordance; Cohen's κ = 0.94; **Fig. 2D–G**). Manual and automated multiplexed-based scores were fully concordant across all samples (31/31 cases; Cohen's κ = 1.0; **Fig. 2F**). One sample was discordant between the multiplexed and original clinical assessment (**Fig. 2D)**. In this case, the original TPS classified the tumor as negative for PD-L1, whereas quantitative multiplexed analysis yielded a TPS of approximately 1.5%, placing the tumor just above the clinical threshold for weak positivity (>1%). Review of the medical records indicated that the patient was initially treated with chemoradiation, subsequently developed recurrent disease, and then received nivolumab (anti PD-1) with a favorable response. Together, these results demonstrate that multiplexed imaging supports accurate and reproducible PD-L1 scoring on a single tissue section, enables objective automated TPS quantification, and facilitates resolution of challenging cases near clinically relevant decision thresholds.

Multiplexed imaging enables detection of clinically actionable biomarkers

We next evaluated whether the multiplexed panel could detect clinically actionable biomarkers relevant for treatment stratification. The panel included antibodies targeting established alterations used in routine clinical practice, such as ALK and ROS1, as well as additional biomarkers of emerging therapeutic relevance, including TROP2, MUC1 and p53 [39–42]. In current workflows, these biomarkers are evaluated using a combination of IHC and molecular assays such as fluorescence *in situ* hybridization (FISH) or next-generation sequencing (NGS). While NGS provides definitive genomic characterization, it typically requires multiple unstained tissue sections and extended turnaround times. This is particularly consequential for alterations such as ALK and ROS1 rearrangements, which are often associated with aggressive disease courses yet predict high response rates to targeted therapies [43–45]. In contrast, IHC detects surrogate changes in protein expression, but is faster. We therefore evaluated whether simultaneous assessment of these targets within the multiplexed assay could provide actionable protein-level information earlier in the diagnostic process.

To assess the accuracy of multiplexed biomarker detection, we compared protein expression in the multiplexed images with available clinical NGS results. All three clinically confirmed ALK-positive tumors were correctly identified as over-expressed by the multiplexed assay (100% concordance, **Fig. 3A-B**). Similarly, all 18 tumors with available p53 or ROS1 status were correctly classified (100% concordance,

Supplementary Fig. 2B-E), showing protein expression patterns consistent with their known genomic alterations. In addition to established biomarkers, multiplexed imaging revealed high expression of TROP2 in 10 tumors and MUC1 in 23 tumors within this cohort (**Fig. 3C-D**). Although these biomarkers are not routinely assessed in standard diagnostic workflows, they are under active clinical investigation as targets for antibody-drug conjugates, including recent regulatory approval of a TROP2-directed therapy for refractory EGFR-mutated NSCLC[46,47], and may serve as biomarkers for ongoing clinical trials[48,49]. TROP2 and MUC1 were frequently co-expressed within the same tumors (n=9), which may have therapeutic implications for patients who could be eligible for multiple agents.

Multiplexed imaging enables evaluation of subcellular protein localization, which is relevant for biomarkers whose therapeutic efficacy depends on target distribution. For TROP2, low membrane-associated expression quantified by the normalized membrane ratio (NMR) has been shown to predict response to TROP2-directed antibody–drug conjugates (ADCs), and recently approved as a companion diagnostic[50]. To evaluate TROP2 localization, we quantified membrane and cytoplasmic signal intensities from multiplexed images and computed an NMR, defined as the fraction of TROP2 signal localized to the membrane (**Fig. 3E-F, Methods**). This metric is conceptually aligned with the previously-described QCS-NMR score for IHC-based TROP2 evaluation[51], but is implemented here using immunofluorescence rather than chromogenic staining. We found that a threshold of 0.6 (closely matching the published QCS-NMR cutoff of 0.56) distinguished membrane-low from membrane-high expression states (**Fig. 3G-H**). Although additional validation is required to establish this approach as a predictive biomarker for TROP2-directed ADCs, these findings suggest that multiplexed imaging can support cell-resolved assessment of target localization.

Together, these results demonstrate that multiplexed imaging enables simultaneous assessment of established and emerging actionable biomarkers within a single tissue section, broadening the treatment-relevant information obtainable from limited biopsy material.

Multiplexed imaging integrates diagnostics and research to enable quantitative analysis of the tumor microenvironment

Finally, we examined whether multiplexed imaging facilitates integration of routine diagnostics with translational research. To this end we incorporated into the panel antibodies to profile the TME, including markers for stromal components, such as CD31, collagen and aSMA, as well as immune cell populations, including CD3, CD20 and CD68. Using InstanSeg [38] for cell segmentation and CellTune [52] for cell classification, we classified cells into 14 major epithelial, stromal, and immune populations across all samples (**Fig. 4A**). This framework enabled generation of a standardized immune-cellular report for each patient, summarizing cell-type abundance and spatial distribution, as well as cohort-level statistics (**Fig.**

4B-C). As an example of quantitative immune profiling, we automatically quantified the fraction of tumor-infiltrating cytotoxic lymphocytes (CD8 TILs) for each patient and observed substantial inter-patient variability (**Fig. 4D–E**). While cytotoxic TILs have been shown to carry prognostic and predictive value in lung cancer beyond PD-L1 TPS [53,54], they are not routinely assessed in clinical practice due to lack of standardized scoring criteria and prospective validation. Here, multiplexed imaging enabled objective, automated cytotoxic TIL quantification directly from diagnostic specimens.

Beyond cytotoxic TILs, multiplexed profiling revealed histology-associated differences in biomarker expression and immune composition. Consistent with prior reports [55–57], MUC1 expression was significantly higher in adenocarcinomas compared with squamous cell carcinomas ($p = 0.0006$), while TROP2 showed a trend toward higher prevalence in squamous carcinomas ($p = 0.107$). Tumors co-expressing both markers did not differ significantly between histologic subtypes (**Fig. 4F**). In addition, squamous cell carcinomas exhibited significantly higher neutrophil fractions than adenocarcinomas ($q = 0.05$), which in turn were higher than those observed in carcinoid tumors, with a similar result when quantifying the fraction of tumor infiltrating neutrophils fractions (TIN) ($q = 0.005$, $q = 0.0169$; **Fig. 4G-H**), consistent with prior observations of subtype-specific immune infiltration patterns [58–60]. Together, these analyses demonstrate that multiplexed imaging offers a scalable framework for generating research-grade insights directly from diagnostic samples, bridging routine diagnostics with translational discovery.

Discussion

Accurate histopathologic diagnosis remains the foundation of precision oncology, particularly in lung cancer, where therapeutic decisions depend on histologic subclassification and biomarker expression. However, current diagnostic workflows are constrained by time-consuming stepwise analyses, small size of biopsies and the tissue-depleting nature of sequential immunohistochemical (IHC) testing. In this study, we show that multiplexed imaging enables tumor classification and biomarker assessment from a single tissue section, achieving diagnostic performance comparable to conventional workflows while directly addressing these limitations.

A central advantage of multiplexed imaging is its ability to expedite diagnostic analyses by replacing serial single-marker testing with simultaneous detection of dozens of clinically relevant markers. In conventional workflows, histologic subtyping, PD-L1 scoring, and assessment of actionable biomarkers are performed sequentially, causing delays in vital treatment [61,62]. In contrast, multiplexed imaging enables many of these assessments to be performed in parallel, supporting earlier treatment decision making. This consideration is particularly consequential in lung cancer, where most patients present with

advanced disease and delays in treatment initiation can adversely affect outcomes [63]. The panel is flexible and easily accommodates integration of new targets (e.g. MET) as they emerge [64].

Multiplexed imaging also conserves limited biopsy material, addressing a persistent challenge in modern diagnostics. Small biopsies are frequently exhausted by serial H&E, IHC, and molecular testing, leading to incomplete diagnosis or biomarker evaluation or repeat invasive procedures. While complementary molecular analysis information may be derived from liquid biopsies, these assays remain costly and further delay treatment initiation. By extracting substantially more information from a single section, multiplexed imaging preserves material for comprehensive molecular profiling, emerging assays, or participation in clinical trials, and reduces the risk of diagnostic failure due to tissue exhaustion. This tissue-sparing property becomes increasingly important as the number of actionable biomarkers continues to expand [65,66].

Beyond efficiency and tissue conservation, multiplexed imaging offers conceptual advantages in diagnostic interpretation through complementary mechanisms. First, evaluating all markers on the same tissue section eliminates the need to infer co-expression and spatial relationships across separate sections, a recognized source of variability that is particularly problematic for low-threshold biomarkers such as PD-L1 [67]. In addition, assessment of multiple lineage and biomarker stains provides contextual information that can resolve diagnostically ambiguous cases. Moreover, multiplexed imaging naturally supports quantitative analysis using automated computational pipelines and facilitates the integration of AI-based tools [68]. This reduces interobserver variability and enables standardized and reproducible biomarker assessment as shown here for automated PD-L1 scoring in NSCLC and machine-learning–based tumor-infiltrating lymphocytes (TIL) quantification studies [69–71].

Importantly, multiplexed imaging also integrates translational and basic research into routine diagnostics without depleting tissue or delaying clinical decision-making. The same assay enables spatially resolved profiling of various markers, generating research-grade data from every diagnostic sample. It also supports investigation of complex biomarkers that depend on multiple co-expressed markers, such as TILs [72,73]. This integration of diagnostics and translational research is particularly relevant as neoadjuvant therapies increasingly limit availability of untreated tumor tissue for research.

Several limitations warrant consideration. For some biomarkers, multiplexed imaging provides protein-level surrogates for genomic alterations, and confirmatory molecular testing remains necessary for definitive genomic characterization in many clinical contexts [74,75]. In addition, successful implementation depends on the availability of antibody clones compatible with multiplexed protocols. For example, EGFR staining could not be reliably optimized in this study, underscoring the need for continued antibody validation and reagent development. Future work should focus on standardizing multiplexed protocols,

validating panels across institutions, ensuring compatibility with digital pathology systems, and evaluating cost-effectiveness and scalability in high-throughput clinical environments. Integration with machine-learning–based analysis and regulatory-grade automation will be essential for widespread adoption.

While this proof-of-concept focuses on lung cancer, the principles demonstrated here are likely applicable to other malignancies characterized by limited tissue or complex phenotyping requirements. Pancreatic and endometrial biopsies, for example, frequently yield minimal tissue [76,77]. The ability to assess multiple co-expressed markers may benefit the diagnosis of lymphomas and other hematologic malignancies in which tumor cells may be relatively scarce and surrounded by an inflammatory infiltrate [78]. Our results suggest that multiplexed imaging may help overcome these challenges by enabling integrated, single-section evaluation of complex marker combinations.

In summary, multiplexed imaging enables fast, tissue-efficient, and accurate diagnostic evaluation while supporting automation and translational research. By consolidating diagnostic and discovery workflows into a single, scalable platform, multiplexed imaging represents a compelling foundation for next-generation pathology in lung cancer and other malignancies characterized by limited tissue and increasing biomarker complexity.

Materials and methods

Experimental model and subject details

A cohort of 109 FFPE archival tissues from patients diagnosed with primary or metastatic lung cancer was obtained from Hadassah Hospital Pathology Department. For the calibration cohort, 55 wedge or lobe resection specimens were reviewed by a board-certified pathologist and representative 2 mm cores were compiled into two tissue microarrays (TMAs). For five of the patients, two cores were included in the TMA (#24, #34, #39, #61, #66), and for one of the patients three cores were included in the TMA (#70), resulting in a total of 62 cores. H&E staining was performed on all cores. For the biopsy validation cohort, 54 biopsies were chosen to include a variety of lung tumors, with varying mutations and PD-L1 scores. H&E-stained slides were obtained from Hadassah Hospital Pathology Department archive.

Data collection

Pathological diagnosis, PD-L1 score, and mutation status were obtained from the medical records.

Staining and imaging

Tissue sections (5 µm thick) were cut from FFPE tissue blocks of the TMA or biopsies using a microtome, and mounted on Superfrost Plus glass slides (Epredia, Netherlands) for staining. Tissue sections were baked at 70°C for 20 min. Tissue sections were deparaffinized with 3 washes of fresh xylene. Tissue sections were then rehydrated with successive washes of ethanol 100% (2x), 95% (2x), 80% (1x), 70% (1x), and DDW (3x). Washes were performed using a Leica ST4020 Linear Stainer (Leica Biosystems, Wetzlar, Germany) programmed to 3 dips per wash for 30 seconds each. The sections were then immersed in epitope retrieval buffer (Target Retrieval Solution, pH 9, DAKO Agilent, Santa Clara, CA) and incubated at 97°C for 40 min and cooled down to 65°C using Lab Vision PT module (Thermo Fisher Scientific, Waltham, MA). Slides were washed for 5 min with a wash buffer made with DDW, 5% of 20X Stock PBS IHC Wash Buffer with Tween 20 (Cell Marque, Rocklin, CA) and 0.1% (w/v) BSA (Thermo Fisher Scientific, Waltham, MA). Tissue sections were stained and imaged using the COMET (Lunaphore, Switzerland) platform according to the manufacturer's recommended protocol. Details on the staining conditions for the primary and secondary antibodies are provided in Supplementary Table 1. Multiplexed images underwent pre-processing within the COMET and subsequently in the Horizon software, as implemented by the manufacturer. Images were registered over imaging cycles and background autofluorescence was removed by subtracting an image of a blank channel. For the TMA, multiplexed image sets were extracted by manually marking individual cores using QuPath's TMA De-arrayer with a diameter of 2.25 mm and a custom Groovy script, which exports them as TIFF files [79].

Diagnosis analysis

Image analysis was performed using QuPath [79]. Paired H&E and multiplexed images derived from the COMET platform were examined in random order by a board-certified pathologist, who was blinded to the original pathological diagnosis during this examination. The diagnoses given by the pathologist were recorded and compared to the original diagnoses. The degree of agreement between the diagnoses obtained using multiplexed imaging and the original diagnoses obtained using conventional IHC was quantified with Cohen's kappa coefficient.

PD-L1 scoring

PD-L1 scores were assigned to each biopsy based on the multiplexed images by a board-certified pathologist and defined as the percentage of viable tumor cells showing membranous PD-L1 staining. PD-L1 scores range between negative (<1% positive cells), weakly positive (1-49% positive cells), and strongly positive (≥50% positive cells) [80]. First, tumor regions were annotated in each biopsy by a pathologist. For the manual PD-L1 scoring, cell segmentation was performed using QuPath's cell detection function, using DAPI as the detection channel. Next, PD-L1-positive tumor cells were manually counted, and scores were calculated as the fraction of positive cells out of all segmented tumor cells. For the automated PD-L1 scoring, cell segmentation was performed using InstanSeg [38] using DAPI for the nuclear staining and PD-L1, CD15, TIGIT, CD20, Calretinin, Synaptophysin, CD31, CD3, CD30, CD8, CD45, HLA-I, IDO-1, MelanA, CD68, Collagen, CK5, CK20, aSMA, PanCK, Podoplanin, and CK7 as membrane markers. Cell type classifiers were created for each tumor type, using QuPath's object classifier, to identify the tumor cells based on a threshold depending on the specific tumor marker. Another classifier was created for PD-L1, using a single threshold for all biopsies. Next, for each tumor type, a composite classifier was created by applying both the tumor and PD-L1 classifiers, resulting in an automated quantification of PD-L1-positive tumor cells. Details on the classifier thresholds are provided in Supplementary Table 1.

TROP2 NMR analysis

Cell segmentation was performed with InstanSeg [38] as described above. Tumor cells were classified using the threshold described above. For each tumor cell, TROP2 mean membrane intensity was calculated as the mean signal ±1μm from the cell segmentation. TROP2 mean cytoplasm intensity was calculated as the mean signal within the eroded cell segmentation (shrunk border -1 μm). NMR score was calculated as $NMR = \frac{TROP2_{mean\ membrane\ intensity}}{TROP2_{mean\ membrane\ intensity} + TROP2_{mean\ cytoplasm\ intensity}}$. NMR threshold was defined as 0.6. $TROP2_{NMR+}$ samples were defined as samples in which $\%Tumor_{NMR \leq 0.6} \geq 75\%$.

Microenvironment analysis

Cell segmentation was performed with InstanSeg[38] as described above. This resulted in 1,734,017 total cells. Tumor and vasculature region masks were generated using the pixel classification module in ilastik[81]. Cells were classified into 14 cell types using CellTune[82]. Cell types and their primary marker definitions are detailed in Supplementary Table 1. Tumor-infiltrating cells were calculated based on the number of cells inside the tumor region masks.

Ethics

All experiments were conducted in accordance with the Declaration of Helsinki and International Ethical Guidelines for Biomedical Research Involving Human Subjects. The use of the human samples was approved by the local ethics committee of Hadassah Medical Center (0250-23-HMO).

Acknowledgements

L.K. holds the Fred and Andrea Fallek President's Development Chair and is supported by the Enoch foundation research fund, the Abisch-Frenkel foundation, the Rising Tide foundation, the Sharon Levine Foundation, Fundación Alberto Palatchi, Dwek center for cancer immunotherapy, and grants from the European Research Council (948811), Israel Science Foundation (2481/20), the Rosetrees Foundation (10004), the Israel Precision Medicine Partnership Program (3830/21), and the Melanoma Research Alliance Team Science Award (1200724). Y.B. is supported by the Clore Scholars Program of the Clore Israel Foundation. E.P. is supported by the Dr. Miriam and Sheldon G. Adelson Medical Research Foundation (AMRF) and the Israel Science Foundation (ISF) Precision Medicine program (1696/20). This study was supported by a grant from the Joint Research Fund of the Hebrew University of Jerusalem and Hadassah Medical Center.

References

1. Siegel RL, Kratzer TB, Giaquinto AN, Sung H, Jemal A. Cancer statistics, 2025. *CA Cancer J Clin*. 2025;75(1):10-45. doi:10.3322/CAAC.21871

2. Howlader N, Forjaz G, Mooradian MJ, et al. The Effect of Advances in Lung-Cancer Treatment on Population Mortality. *New England Journal of Medicine*. 2020;383(7):640-649. doi:10.1056/NEJMOA1916623,

3. Wang Z, Cai G, Zhu J, Wang J, Zhang Y. Treatment of advanced-stage non-small cell lung cancer: Current progress and a glimpse into the future (Review). *Mol Clin Oncol*. 2025;22(5). doi:10.3892/MCO.2025.2837,

4. Ramalingam SS, Vansteenkiste J, Planchard D, et al. Overall Survival with Osimertinib in Untreated, EGFR -Mutated Advanced NSCLC . *New England Journal of Medicine*. 2020;382(1):41-50. doi:10.1056/NEJMOA1913662/SUPPL_FILE/NEJMOA1913662_DATA-SHARING.PDF

5. Mok T, Camidge DR, Gadgeel SM, et al. Updated overall survival and final progression-free survival data for patients with treatment-naive advanced ALK-positive non-small-cell lung cancer in the ALEX study. *Annals of Oncology*. 2020;31(8):1056-1064. doi:10.1016/j.annonc.2020.04.478

6. Gandhi L, Rodríguez-Abreu D, Gadgeel S, et al. Pembrolizumab plus Chemotherapy in Metastatic Non-Small-Cell Lung Cancer. *N Engl J Med*. 2018;378(22):2078-2092. doi:10.1056/NEJMOA1801005

7. Paz-Ares L, Ciuleanu TE, Cobo M, et al. First-line nivolumab plus ipilimumab combined with two cycles of chemotherapy in patients with non-small-cell lung cancer (CheckMate 9LA): an international, randomised, open-label, phase 3 trial. *Lancet Oncol*. 2021;22(2):198-211. doi:10.1016/S1470-2045(20)30641-0

8. Solomon BJ, Bauer TM, Mok TSK, et al. Efficacy and safety of first-line lorlatinib versus crizotinib in patients with advanced, ALK-positive non-small-cell lung cancer: updated analysis of data from the phase 3, randomised, open-label CROWN study. *Lancet Respir Med*. 2023;11(4):354-366. doi:10.1016/S2213-2600(22)00437-4

9. Hall H, Tocock A, Burdett S, et al. Association between time-to-treatment and outcomes in non-small cell lung cancer: a systematic review. *Thorax*. 2022;77(8):762-768. doi:10.1136/THORAXJNL-2021-216865,

10. Zer A, Ahn MJ, Barlesi F, et al. Early and locally advanced non-small-cell lung cancer: ESMO Clinical Practice Guideline for diagnosis, treatment and follow-up. *Ann Oncol*. 2025;36(11). doi:10.1016/J.ANNONC.2025.08.003

11. Hendriks LE, Kerr KM, Menis J, et al. Oncogene-addicted metastatic non-small-cell lung cancer: ESMO Clinical Practice Guideline for diagnosis, treatment and follow-up☆. *Annals of Oncology*. 2023;34(4):339-357. doi:10.1016/j.annonc.2022.12.009

12. Yatabe Y, Dacic S, Borczuk AC, et al. Best Practices Recommendations for Diagnostic Immunohistochemistry in Lung Cancer. *J Thorac Oncol*. 2018;14(3):377. doi:10.1016/J.JTHO.2018.12.005

13. Righi L, Graziano P, Fornari A, et al. Immunohistochemical subtyping of nonsmall cell lung cancer not otherwise specified in fine-needle aspiration cytology: A retrospective study of 103 cases with surgical

correlation. *Cancer*. 2011;117(15):3416-3423. doi:10.1002/CNCR.25830;PAGEGROUP:STRING:PUBLICATION

14. Liam CK, Mallawathantri S, Fong KM. Is tissue still the issue in detecting molecular alterations in lung cancer? *Respirology*. 2020;25(9):933-943. doi:10.1111/RESP.13823

15. Tsao MS, Kerr KM, Kockx M, et al. PD-L1 Immunohistochemistry Comparability Study in Real-Life Clinical Samples: Results of Blueprint Phase 2 Project. *J Thorac Oncol*. 2018;13(9):1302. doi:10.1016/J.JTHO.2018.05.013

16. Mino-Kenudson M, Schalper K, Cooper W, et al. Predictive Biomarkers for Immunotherapy in Lung Cancer: Perspective From the International Association for the Study of Lung Cancer Pathology Committee. *Journal of Thoracic Oncology*. 2022;17(12):1335-1354. doi:10.1016/J.JTHO.2022.09.109

17. Thiele B, Ding L, Sorenson A, Huang Y, Clinic M, Rochester. Optimizing Tissue Adequacy for Molecular Testing in Small Biopsies for Primary Lung Neoplasms: A Root Cause Analysis and Proposed Solutions. *J Am Soc Cytopathol*. 2024;13(5):S46-S47. doi:10.1016/J.JASC.2024.08.084

18. Hoang TCT, Debieuvre D, Bravard AS, et al. Risk factors for early mortality from lung cancer: evolution over the last 20 years in the French nationwide KBP cohorts. *ESMO Open*. 2024;9(6):103594. doi:10.1016/J.ESMOOP.2024.103594

19. Grivaux M, Debieuvre D, Herman D, et al. Early mortality in lung cancer: French prospective multicentre observational study. *BMC Pulm Med*. 2016;16(1). doi:10.1186/S12890-016-0205-5,

20. Fleming KE, Hupel A, Mithoowani H, Lulic-Kuryllo T, Valdes M. Biomarker Turnaround Times and Impact on Treatment Decisions in Patients with Advanced Non-Small Cell Lung Carcinoma at a Large Canadian Community Hospital with an Affiliated Regional Cancer Centre. *Current Oncology*. 2024;31(3):1515. doi:10.3390/CURRONCOL31030115

21. Stewart DJ, Maziak DE, Moore SM, et al. The need for speed in advanced non-small cell lung cancer: A population kinetics assessment. *Cancer Med*. 2021;10(24):9040-9046. doi:10.1002/CAM4.4411

22. Hormalainen K, Marttila K, Nykter M, et al. Comprehensive Genomic Profiling in Advanced Non-Small Cell Lung Cancer: A Real-World Cohort Study in Finland. *Cancer Med*. 2025;14(19):e71250. doi:10.1002/CAM4.71250

23. Takeda M, Takahama T, Sakai K, et al. Clinical Application of the FoundationOne CDx Assay to Therapeutic Decision-Making for Patients with Advanced Solid Tumors. *Oncologist*. 2021;26(4):e588. doi:10.1002/ONCO.13639

24. Lin JR, Chen YA, Campton D, et al. High-plex immunofluorescence imaging and traditional histology of the same tissue section for discovering image-based biomarkers. *Nature Cancer 2023 4:7*. 2023;4(7):1036-1052. doi:10.1038/s43018-023-00576-1

25. Koomen BM, Voorham QJM, Epskamp-Kuijpers CCHJ, et al. Considerable interlaboratory variation in PD-L1 positivity in a nationwide cohort of non-small cell lung cancer patients. *Lung Cancer*. 2021;159:117-126. doi:10.1016/J.LUNGCAN.2021.07.012

26. Marletta S, Fusco N, Munari E, et al. Atlas of PD-L1 for Pathologists: Indications, Scores, Diagnostic Platforms and Reporting Systems. *J Pers Med*. 2022;12(7). doi:10.3390/JPM12071073

27. Forde PM, Spicer JD, Provencio M, et al. Overall Survival with Neoadjuvant Nivolumab plus Chemotherapy in Lung Cancer. *New England Journal of Medicine*. 2025;393(8):741-752. doi:10.1056/NEJMOA2502931;ISSUE:ISSUE:DOI

28. Hu J, Zhang J, Wan S, Zhang P. Neoadjuvant immunotherapy for non-small cell lung cancer: Opportunities and challenges. *Chinese Medical Journal Pulmonary and Critical Care Medicine*. 2024;2(4):224-239. doi:10.1016/J.PCCM.2024.11.003

29. Wakelee H, Liberman M, Kato T, et al. Perioperative Pembrolizumab for Early-Stage Non-Small-Cell Lung Cancer. *N Engl J Med*. 2023;389(6):491-503. doi:10.1056/NEJMOA2302983

30. Hines JB, Cameron RB, Esposito A, et al. Evaluation of Major Pathologic Response and Pathologic Complete Response as Surrogate End Points for Survival in Randomized Controlled Trials of Neoadjuvant Immune Checkpoint Blockade in Resectable in NSCLC. *J Thorac Oncol*. 2024;19(7):1108-1116. doi:10.1016/J.JTHO.2024.03.010

31. La Salvia A, Meyer ML, Hirsch FR, et al. Rediscovering immunohistochemistry in lung cancer. *Crit Rev Oncol Hematol*. 2024;200:104401. doi:10.1016/J.CRITREVONC.2024.104401

32. Harms PW, Frankel TL, Moutafi M, et al. Multiplex Immunohistochemistry and Immunofluorescence: A Practical Update for Pathologists. *Modern Pathology*. 2023;36(7):100197. doi:10.1016/J.MODPAT.2023.100197/ASSET/17465717-0F27-4CE1-93FE-045E2526AFCF/MAIN.ASSETS/FIGS4.JPG

33. Pennell NA, Arcila ME, Gandara DR, West H. Biomarker Testing for Patients With Advanced Non–Small Cell Lung Cancer: Real-World Issues and Tough Choices. *American Society of Clinical Oncology Educational Book*. 2019;(39):531-542. doi:10.1200/EDBK_237863/ASSET/D5DFC14C-E5EB-404F-9614-4A1676D0BBDD/ASSETS/IMAGES/LARGE/EDBK_237863_FIG3.JPG

34. Roberts EA, Morrison LE, Behman LJ, Draganova-Tacheva R, O'Neill R, Solomides CC. Chromogenic immunohistochemical quadruplex provides accurate diagnostic differentiation of non-small cell lung cancer. *Ann Diagn Pathol*. 2020;45. doi:10.1016/j.anndiagpath.2019.151454

35. Ilié M, Beaulande M, Long-Mira E, et al. Analytical validation of automated multiplex chromogenic immunohistochemistry for diagnostic and predictive purpose in non-small cell lung cancer. *Lung Cancer*. 2022;166:1-8. doi:10.1016/j.lungcan.2022.01.022

36. van den Brand M, Hoevenaars BM, Sigmans JHM, et al. Sequential immunohistochemistry: a promising new tool for the pathology laboratory. *Histopathology*. 2014;65(5):651-657. doi:10.1111/HIS.12446

37. Rivest F, Eroglu D, Pelz B, et al. Fully automated sequential immunofluorescence (seqIF) for hyperplex spatial proteomics. *Sci Rep*. 2023;13(1):1-14. doi:10.1038/S41598-023-43435-W;SUBJMETA=1257,1647,2225,245,327,631,664,67;KWRD=CANCER+MICROENVIRONMENT,FLUORESCENCE+IMAGING,IMMUNOHISTOCHEMISTRY

38. Goldsborough T, Philps B, O'Callaghan A, et al. InstanSeg: an embedding-based instance segmentation algorithm optimized for accurate, efficient and portable cell segmentation. Published online August 28, 2024. Accessed January 2, 2026. https://arxiv.org/pdf/2408.15954

39. Li XX, Chen JL. TROP2: as a promising target in lung cancer. *Front Oncol*. 2025;15:1569897. doi:10.3389/FONC.2025.1569897

40. Grewal US, Kurzrock R. Mucin-1: a promising pan-cancer therapeutic target. *npj Precision Oncology 2025 9:1*. 2025;9(1):218-. doi:10.1038/s41698-025-01016-2

41. Huang X, Sun Q, Chen C, et al. MUC1 overexpression predicts worse survival in patients with non-small cell lung cancer: evidence from an updated meta-analysis. *Oncotarget*. 2017;8(52):90315. doi:10.18632/ONCOTARGET.19861

42. Zhang C, Yang C, Shi Q. Effects of Tp53 Gene Mutations on the Survival of Non-Small Cell Lung Cancer (NSCLC); A Short Review. *Cancer Manag Res*. 2025;17:65. doi:10.2147/CMAR.S495006

43. Bischoff H, Gendarme S, Somme L, Chouaid C, Schott R. Evolving Therapeutic Landscape of ROS1-Positive Non-Small Cell Lung Cancer: An Updated Review. *Curr Oncol*. 2025;32(11). doi:10.3390/CURRONCOL32110626

44. Schneider JL, Lin JJ, Shaw AT. ALK-positive lung cancer: a moving target. *Nat Cancer*. 2023;4(3):330-343. doi:10.1038/S43018-023-00515-0

45. Griesinger F, Roeper J, Pöttgen C, Willborn KC, Eberhardt WEE. Brain metastases in ALK-positive NSCLC - time to adjust current treatment algorithms. *Oncotarget*. 2018;9(80):35181-35194. doi:10.18632/ONCOTARGET.26073

46. Sands J, Ahn MJ, Lisberg A, et al. Datopotamab Deruxtecan in Advanced or Metastatic Non-Small Cell Lung Cancer With Actionable Genomic Alterations: Results From the Phase II TROPION-Lung05 Study. *J Clin Oncol*. 2025;43(10):1254-1265. doi:10.1200/JCO-24-01349

47. Ahn MJ, Tanaka K, Paz-Ares L, et al. Datopotamab Deruxtecan Versus Docetaxel for Previously Treated Advanced or Metastatic Non-Small Cell Lung Cancer: The Randomized, Open-Label Phase III TROPION-Lung01 Study. *J Clin Oncol*. 2025;43(3):260-272. doi:10.1200/JCO-24-01544

48. Patel SP, Gadgeel S, Mino-Kenudson M, Naidoo J, Sethakorn N. Clinical overview of trophoblast surface antigen 2 Antibody-Drug conjugates in Non–Small cell lung cancer. *Cancer Treat Rev*. Published online November 16, 2025:103050. doi:10.1016/J.CTRV.2025.103050

49. Takano K, Yukiura M, Takahashi K, et al. DS-3939a: A TA-MUC1-Directed Antibody-Drug Conjugate with Broad Antitumor Activity. *Mol Cancer Ther*. 2026;25(1):OF1-OF14. doi:10.1158/1535-7163.MCT-24-0666

50. Roche granted FDA Breakthrough Device Designation for first AI-driven companion diagnostic for non-small cell lung cancer. Accessed January 18, 2026. https://www.roche.com/media/releases/med-cor-2025-04-29

51. Garassino MC, Sands J, Paz-Ares L, et al. PL02.11 Normalized Membrane Ratio of TROP2 by Quantitative Continuous Scoring is Predictive of Clinical Outcomes in TROPION-Lung 01. *Journal of Thoracic Oncology*. 2024;19(10):S2-S3. doi:10.1016/J.JTHO.2024.09.015

52. Bussi Y, Shainshein D, Ovits E, et al. CellTune: An integrative software for accurate cell classification in spatial proteomics. *bioRxiv*. Published online May 9, 2025:2025.05.05.652215. doi:10.1101/2025.05.05.652215

53. Alessi J V., Lindsay JR, Giobbie-Hurder A, et al. Immunoprofiling at an Institutional Scale Reveals That High Numbers of Intratumoral CD8+ and PD-1+ Cells Predict Superior Patient Survival Across Major Cancer Types Independent of Major Risk Factors. *JCO Precis Oncol*. 2025;9(9):e2500240. doi:10.1200/PO-25-00240

54. Cheng C, Nguyen TT, Tang M, et al. Immune Infiltration in Tumor and Adjacent Non-Neoplastic Regions Codetermines Patient Clinical Outcomes in Early-Stage Lung Cancer. *Journal of Thoracic Oncology*. 2023;18(9):1184-1198. doi:10.1016/j.jtho.2023.04.022

55. Situ D, Wang J, Ma Y, et al. Expression and prognostic relevance of MUC1 in stage IB non-small cell lung cancer. *Med Oncol*. 2011;28 Suppl 1(SUPPL. 1). doi:10.1007/S12032-010-9752-4

56. Lan Y, Ni W, Tai G. Expression of MUC1 in different tumours and its clinical significance (Review). *Mol Clin Oncol*. 2022;17(6). doi:10.3892/MCO.2022.2594

57. Inamura K, Yokouchi Y, Kobayashi M, et al. Association of tumor TROP2 expression with prognosis varies among lung cancer subtypes. *Oncotarget*. 2017;8(17):28725-28735. doi:10.18632/ONCOTARGET.15647

58. Wu F, Fan J, He Y, et al. Single-cell profiling of tumor heterogeneity and the microenvironment in advanced non-small cell lung cancer. *Nat Commun*. 2021;12(1). doi:10.1038/S41467-021-22801-0

59. Salcher S, Sturm G, Horvath L, et al. High-resolution single-cell atlas reveals diversity and plasticity of tissue-resident neutrophils in non-small cell lung cancer. *Cancer Cell*. 2022;40(12):1503-1520.e8. doi:10.1016/J.CCELL.2022.10.008

60. Horvath L, Puschmann C, Scheiber A, et al. Beyond binary: bridging neutrophil diversity to new therapeutic approaches in NSCLC. *Trends Cancer*. 2024;10(5):457-474. doi:10.1016/J.TRECAN.2024.01.010

61. Lindquist KE, Gudinaviciene I, Mylona N, et al. Real-World Diagnostic Accuracy and Use of Immunohistochemical Markers in Lung Cancer Diagnostics. *Biomolecules*. 2021;11(11). doi:10.3390/BIOM11111721

62. Patel S, Smith JB, Kurbatova E, Guarner J. Factors that impact turnaround time of surgical pathology specimens in an academic institution. *Hum Pathol*. 2012;43(9):1501-1505. doi:10.1016/j.humpath.2011.11.010

63. Romine PE, Sun Q, Fedorenko C, et al. Impact of Diagnostic Delays on Lung Cancer Survival Outcomes: A Population Study of the US SEER-Medicare Database. *JCO Oncol Pract*. 2022;18(6):e877-e885. doi:10.1200/OP.21.00485

64. Camidge DR, Bar J, Horinouchi H, et al. Telisotuzumab Vedotin Monotherapy in Patients With Previously Treated c-Met Protein-Overexpressing Advanced Nonsquamous EGFR-Wildtype Non-Small Cell Lung Cancer in the Phase II LUMINOSITY Trial. *J Clin Oncol*. 2024;42(25):3000-3011. doi:10.1200/JCO.24.00720

65. Chiari R, Sidoni A, Metro G. Early stage resectable non-small cell lung cancer: is neoadjuvant immunotherapy the right way forward? *J Thorac Dis*. 2018;10(Suppl 33):S3890. doi:10.21037/JTD.2018.10.22

66. Weissferdt A, Leung CH, Lin H, et al. Pathologic Processing of Lung Cancer Resection Specimens After Neoadjuvant Therapy. *Mod Pathol*. 2024;37(1). doi:10.1016/J.MODPAT.2023.100353

67. Lu S, Stein JE, Rimm DL, et al. Comparison of Biomarker Modalities for Predicting Response to PD-1/PD-L1 Checkpoint Blockade: A Systematic Review and Meta-analysis. *JAMA Oncol*. 2019;5(8):1195-1204. doi:10.1001/JAMAONCOL.2019.1549

68. Arnon J, Dinstag G, Tirosh O, et al. Predictive value of ENLIGHT-DP in patients with metastatic lung adenocarcinoma treated with immune checkpoint inhibitors and platinum chemotherapy directly from histopathology slides using inferred transcriptomics. *J Immunother Cancer*. 2025;13(1). doi:10.1136/JITC-2024-010132

69. Plass M, Olteanu GE, Dacic S, et al. Comparative performance of PD-L1 scoring by pathologists and AI algorithms. *Histopathology*. 2025;87(1):90-100. doi:10.1111/HIS.15432

70. Aung TN, Liu M, Su D, et al. Pathologist-Read vs AI-Driven Assessment of Tumor-Infiltrating Lymphocytes in Melanoma. *JAMA Netw Open*. 2025;8(7):e2518906-e2518906. doi:10.1001/JAMANETWORKOPEN.2025.18906

71. Barnes M, Srinivas C, Bai I, et al. Whole tumor section quantitative image analysis maximizes between-pathologists' reproducibility for clinical immunohistochemistry-based biomarkers. *Laboratory Investigation*. 2017;97(12):1508-1515. doi:10.1038/labinvest.2017.82

72. Lin JR, Chen YA, Campton D, et al. High-plex immunofluorescence imaging and traditional histology of the same tissue section for discovering image-based biomarkers. *Nature Cancer 2023 4:7*. 2023;4(7):1036-1052. doi:10.1038/s43018-023-00576-1

73. Kuehl M, Okabayashi Y, Wong MN, et al. Pathology-oriented multiplexing enables integrative disease mapping. *Nature 2025 644:8076*. 2025;644(8076):516-526. doi:10.1038/s41586-025-09225-2

74. Conde E, Rojo F, Gómez J, et al. Molecular diagnosis in non-small-cell lung cancer: expert opinion on ALK and ROS1 testing. *J Clin Pathol*. 2022;75(3):145-153. doi:10.1136/JCLINPATH-2021-207490

75. Lindeman NI, Cagle PT, Aisner DL, et al. Updated Molecular Testing Guideline for the Selection of Lung Cancer Patients for Treatment With Targeted Tyrosine Kinase Inhibitors: Guideline From the College of American Pathologists, the International Association for the Study of Lung Cancer, and the…. *Arch Pathol Lab Med*. 2018;142(3):321-346. doi:10.5858/ARPA.2017-0388-CP

76. Lai JH, Lin CC, Ho KC, Chang CW. Impact of tumor type and size on macroscopic tissue core retrieval in endoscopic ultrasound-guided fine needle biopsy for pancreatic malignancies. *BMC Gastroenterol*. 2024;24(1). doi:10.1186/S12876-024-03517-Z

77. Reijnen C, Visser NCM, Bulten J, Massuger LFAG, Van Der Putten LJM, Pijnenborg JMA. Diagnostic accuracy of endometrial biopsy in relation to the amount of tissue. *J Clin Pathol*. 2017;70(11):941-946. doi:10.1136/JCLINPATH-2017-204338

78. Liu J, Lau SK, Varma VA, Kairdolf BA, Nie S. Multiplexed Detection and Characterization of Rare Tumor Cells in Hodgkin's Lymphoma with Multicolor Quantum Dots. *Anal Chem*. 2010;82(14):6237-6243. doi:10.1021/AC101065B

79. Bankhead P, Loughrey MB, Fernández JA, et al. QuPath: Open source software for digital pathology image analysis. *Scientific Reports 2017 7:1*. 2017;7(1):16878-. doi:10.1038/s41598-017-17204-5

80. Sholl LM, Awad M, Roy UB, et al. Programmed Death Ligand-1 and Tumor Mutation Burden Testing of Patients With Lung Cancer for Selection of Immune Checkpoint Inhibitor Therapies: Guideline From the College of American Pathologists, Association for Molecular Pathology, International Association for the Study of Lung Cancer, Pulmonary Pathology Society, and LUNGevity Foundation. *Arch Pathol Lab Med*. 2024;148(7):757-774. doi:10.5858/ARPA.2023-0536-CP

81. Berg S, Kutra D, Kroeger T, et al. ilastik: interactive machine learning for (bio)image analysis. *Nature Methods 2019 16:12*. 2019;16(12):1226-1232. doi:10.1038/s41592-019-0582-9

82. Bussi Y, Shainshein D, Ovits E, et al. CellTune: An integrative software for accurate cell classification in spatial proteomics. *bioRxiv*. Published online May 9, 2025:2025.05.05.652215. doi:10.1101/2025.05.05.652215

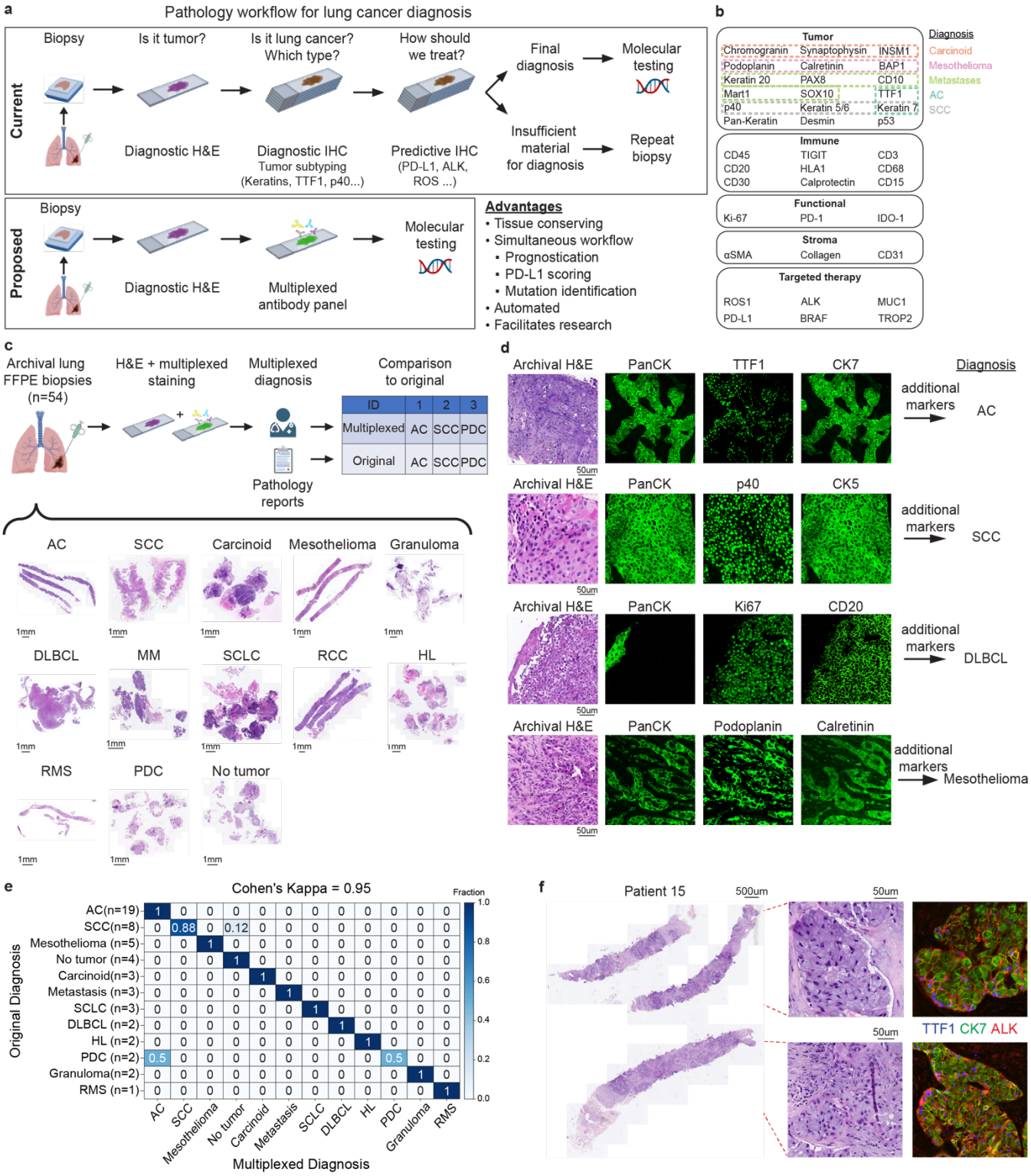

Figure 1: Multiplexed imaging enables accurate classification of biopsies

(a) Conventional immunohistochemistry workflow (top) vs. multiplexed imaging-based workflow (bottom). **(b)** 39-plex antibody panel designed for diagnosis, biomarker evaluation, mutation identification, and immune composition analysis. **(c)** Lung FFPE biopsies were stained for H&E and multiplexed imaging, and diagnosed. Results were compared to the original diagnoses. **(d)** Representative cases demonstrating multiple immunofluorescent stains in addition to H&E, leading to a final diagnosis. **(e)** Agreement between multiplexed-based diagnosis (x-axis) and the original diagnosis (y-axis). Color depicts fraction of cases per row. **(f)** Diagnosed poorly differentiated carcinoma showing ALK expression in the multiplexed image. Abbreviations: AC = Adenocarcinoma, SCC = Squamous cell carcinoma, MM = Malignant melanoma, DLBCL = Diffuse large B-cell lymphoma, SCLC = Small cell lung carcinoma, RCC = Renal cell carcinoma, HL = Hodgkin lymphoma, RMS = Rhabdomyosarcoma, PDC = Poorly differentiated carcinoma.

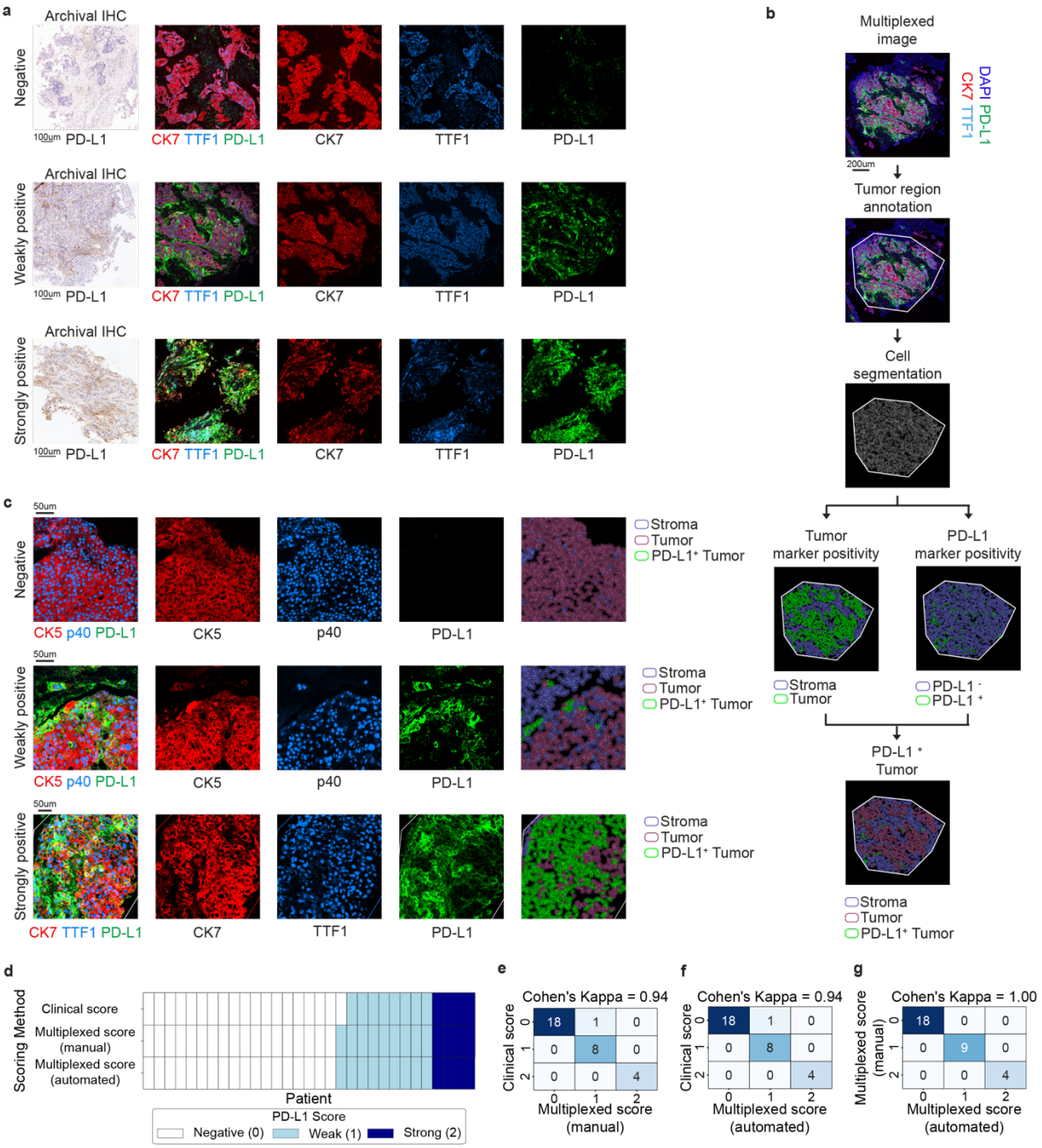

Figure 2: Multiplexed imaging enables accurate manual and automated PD-L1 scoring

(a) Representative cases demonstrating manual PD-L1 TPS scoring of negative (<1%, top), weakly positive (1-49%, middle), and strongly positive (≥50%, bottom) tumors, in addition to the original PD-L1 IHC stains. **(b)** Workflow for automated PD-L1 scoring using multiplexed images and marker positivity. A pathologist annotates the tumor regions, followed by cell segmentation based on nuclear staining. Next, tumor and PD-L1 marker positivity are determined using a threshold classifier. Finally PD-L1-positive tumor cells are determined as the intersection between the two classifiers. **(c)** Representative cases demonstrating automated PD-L1 TPS scoring of negative (<1%, top), weakly positive (1-49%, middle), and strongly positive (≥50%, bottom) tumors. Stroma (blue), PD-L1 negative tumor (light red), PD-L1 positive cells (green). **(d)** PD-L1 scoring method (y-axis) tile map by patients (x-axis). PD-L1 scores: 0 = Negative, 1 = Weakly positive, 2 = Strongly positive. **(e)** Confusion between the original PD-L1 score (y-axis) and manual multiplexed score (x-axis). Color indicates number of cases. **(f)** Confusion between the original PD-L1 score (y-axis) and automated multiplexed score (x-axis). Color indicates number of cases. **(g)** Confusion between the manual multiplexed PD-L1 score (y-axis) and automated multiplexed score (x-axis). Color indicates number of cases.

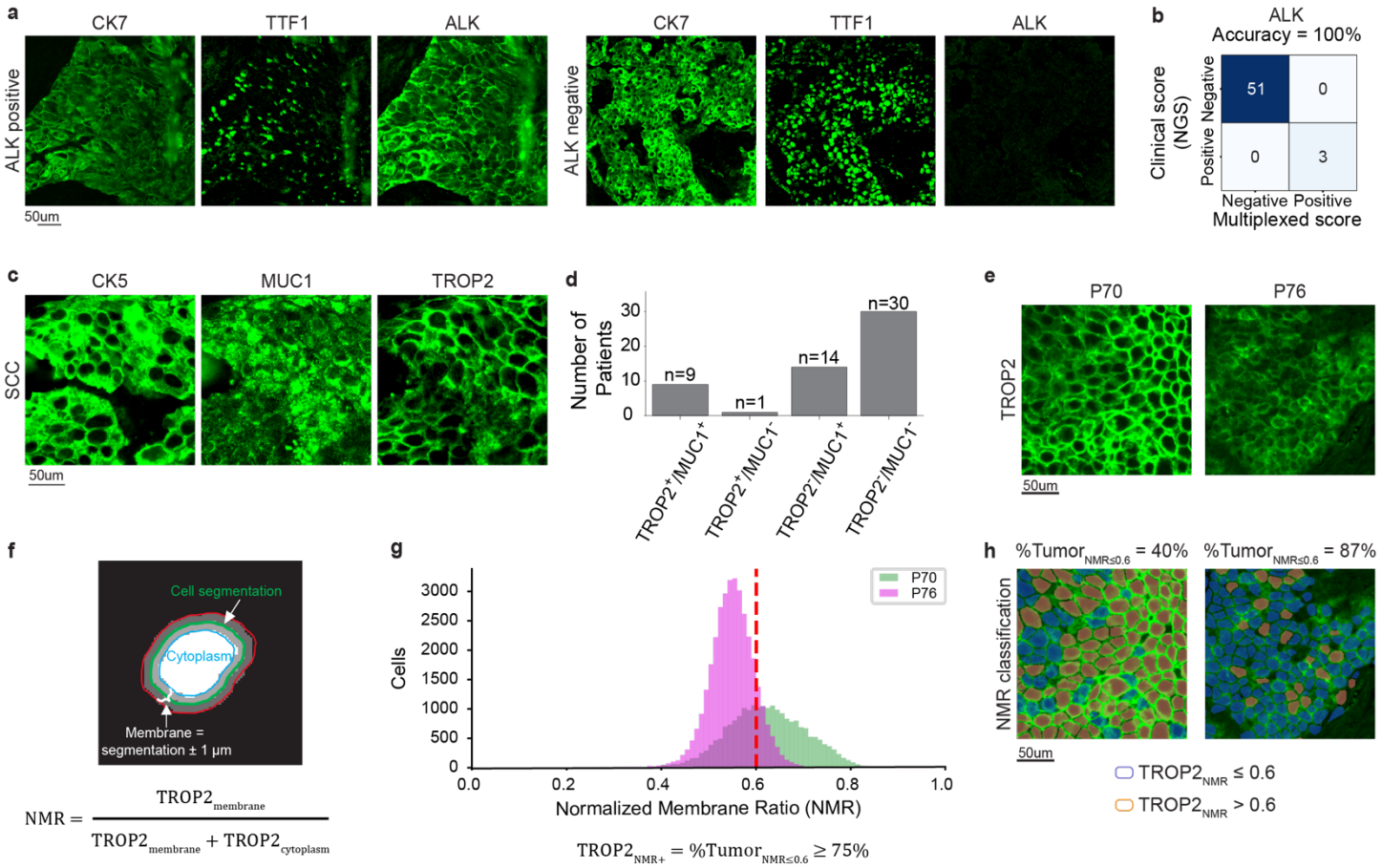

Figure 3: Multiplexed imaging enables detection of clinically actionable biomarkers and mutations

(a) Representative images of ALK positive (left) and negative (right) tumors. **(b)** Confusion between NGS (y-axis) and multiplexed imaging (x-axis) in detecting ALK mutation. Color indicates number of cases. **(c)** Representative image of $TROP2^{+}/MUC1^{+}$ squamous cell carcinoma. **(d)** Bar graph of TROP2 and MUC1 expression (x-axis) across patients (y-axis). **(e)** Representative images of TROP2-positive patients with two distinct expression patterns. **(f)** NMR (Normalized Membrane Ratio) calculation for TROP2 expression was done using TROP2 membrane measurement (±1µm cell segmentation) and TROP2 cytoplasm measurement. **(g)** Cells count (y-axis) NMR distribution (x-axis) of patients 70 (green) and 76 (magenta). TROP2-NMR+ was defined as tumors with ≥ 75% of cell with TROP2-NMR ≤0.6. **(h)** Same as e, but with NMR classification. Blue = TROP2-NMR ≤ 0.6, red = TROP2-NMR > 0.6.

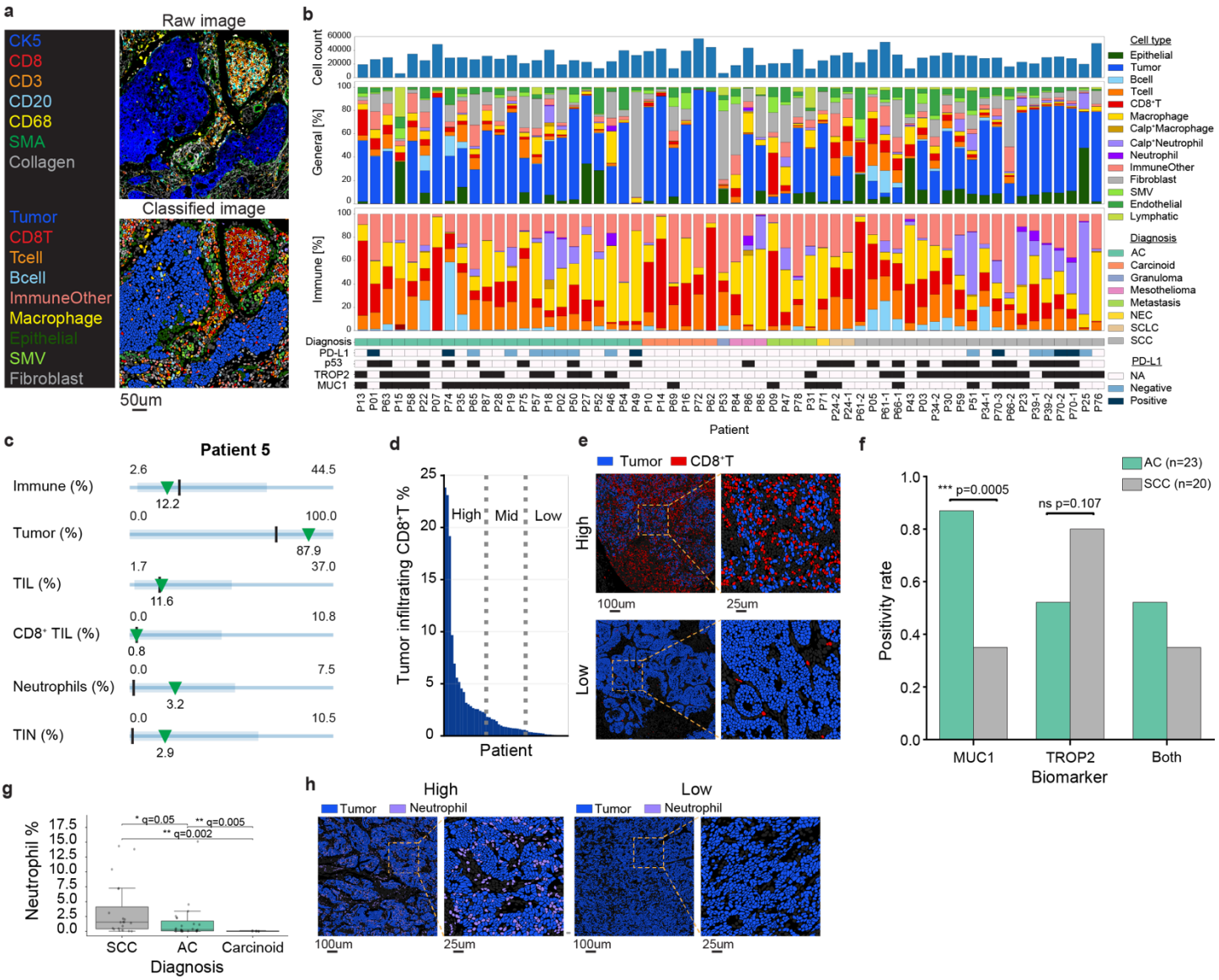

Figure 4: Multiplexed imaging enables quantitative analysis of the tumor microenvironment

(a) Protein expression images (top) are used to generate cell-type classifications (bottom) for downstream quantitative analysis. **(b)** Top: total number of cells and their relative abundances (y-axis) across all patients (x-axis) according to tumor subtypes. Middle: the same for immune cells only. Bottom: tumor characteristics per patient. Black is positive for biomarker. **(c)** Example of a standardized cellular report for one patient. Green triangles indicate the patient's value, black lines indicate the median across patients, blue lines indicate the full range across patients and the thick blue lines indicate 5th-95th percentile. **(d)** Stratification of patients (x-axis) into tertiles according to $CD8^+$ T-cell infiltration (y-axis). **(e)** Representative cell classification images of patients with high (top) and low (bottom) $CD8^+$ T-cell infiltration. Tumor cells (blue), $CD8^+$ T cells (red), other cell types (gray). **(f)** Positivity rate (y-axis) of MUC1 (left), TROP2 (middle), and both (right) in adenocarcinomas (AC) and squamous cell carcinomas (SCC). Statistical significance was assessed using Fisher's exact test. **(g)** Fraction of neutrophils (y-axis) in squamous cell carcinomas (SCC), adenocarcinomas (AC), and typical carcinoid (TC) tumors (x-axis) with Mann Whitney q values (FDR corrected p values). **(h)** Representative cell classification images of patients with high (top) and low (bottom) neutrophil %. Tumor cells (blue), neutrophils (magenta), other cell types (gray). Abbreviations: AC = Adenocarcinoma, NEC = Neuroendocrine carcinoma, SCLC = Small cell lung carcinoma, SCC = Squamous cell carcinoma.